IEEE Access
Multidisciplinary | Rapid Review | Open Access Journal

Received 28 February 2024, accepted 20 March 2024, date of publication 27 March 2024, date of current version 2 April 2024.

Digital Object Identifier 10.1109/ACCESS.2024.3381519

RESEARCH ARTICLE

Ultra High-Speed Fault Diagnosis Scheme for DC Distribution Systems Based on Discrete Median Filter and Mathematical Morphology

FAISAL MUMTAZ[1], TAHA SAEED KHAN[2], MOHAMMED ALQAHTANI[3], (Member, IEEE), HADEED AHMED SHER[4], (Senior Member, IEEE), ALI S. ALJUMAH[3], AND SULAIMAN Z. ALMUTAIRI[3]

[1]USPCAS-E, National University of Sciences and Technology (NUST), Islamabad 44000, Pakistan
[2]School of Electrical and Computer Engineering, Oklahoma State University, Stillwater, OK 74078, USA
[3]Electrical Engineering Department, College of Engineering, Prince Sattam Bin Abdulaziz University, Al-Kharj 11942, Saudi Arabia
[4]Faculty of Electrical Engineering, Ghulam Ishaq Khan Institute of Engineering Sciences and Technology, Topi 23640, Pakistan

Corresponding author: Faisal Mumtaz (fmumtazphd21.ces@student.nust.edu.pk)

The authors extend their appreciation to Prince Sattam Bin Abdulaziz University for funding this research work through the project number (PSAU/2023/01/9076).

ABSTRACT In the modern world, the growing presence of renewable energy power near the consumer end makes DC distribution systems more attractive than traditional AC ones. However, designing fault diagnosis schemes for the DC distribution system is a complicated problem due to noisy measurements and rapidly rising DC-fault currents. This article proposes an Ultra High-speed Fault Diagnosis scheme using a Discrete Median Filter and Mathematical Morphology Algorithm. In the first stage, the acquired current signal from a corresponding faulty bus is preprocessed using a Discrete Median Filter for state estimation and noise reduction. In the second stage, the proposed Scheme computes the DC Residual by deploying the Mathematical Morphology Algorithm on the DMF estimated current signal. The DC Residual represents the mathematical computed difference between the filtered output of the Mathematical Morphology Algorithm and the Discrete Median Filter-estimated current signal. Then, the proposed method cross-matches variations in the computed DC Residual with pre-defined threshold settings to detect faults successfully and promptly. In the third stage, the Mathematical Morphology Algorithm-based Energy is computed for fault classification and section identification. The polarity of Mathematical Morphology Algorithm-based Energy is used to categorize and locate all types of DC faults in the proposed scheme. The suggested method is tested on a DC distribution test bed via MATLAB/Simulink 2022b. The results demonstrate that the suggested scheme successfully identifies all types of DC faults in less than 2.5 msec, with 99% accuracy.

INDEX TERMS Discrete median filter, fault detection, mathematical morphology, renewable energy-based DC distribution network, smart grids.

NOMENCLATURE

Alternating current	AC.
Artificial intelligence	AI.
Circuit breaker	CB.
DC-residuals	DCR.
Discrete Median Filter	DMF.
Direct current	DC.
DC distribution system	DCDS.
Electric vehicles	EV.
Energy storage systems	ESS.
Empirical-mode decomposition	EMD.
Kalman filter	KF.
Mathematical Morphology Algorithm	MMA.
Medium voltage DC	MVDC.
Mathematical Morphology Algorithm-based Energy	MMABE.
Machine learning	ML.
Protection relay	PR.
Phasor measurement units	PMUs.
Ultra High-speed Fault Diagnosis Scheme	UHSFD.
Support vector machine	SVM.

The associate editor coordinating the review of this manuscript and approving it for publication was Mehrdad Saif.

I. INTRODUCTION

The increasing electricity demand is coupled with the limited capacity of existing AC distribution systems which leads to a growing interest in alternative power distribution technologies [1]. One such alternative is the DCDS, which has gained considerable attention in recent years [2], [3]. Unlike conventional AC systems, the DCDS offers several advantages [1], [4], [5], including higher efficiency, lower losses, enhanced integration of renewable energy sources, and facilitated DC-based applications. With the increasing adoption of DC-based devices and the advancement of power electronics technology, the DCDS has emerged as a promising solution for future power distribution [4], [6], [7]. However, fault detection in the DCDS is crucial to ensure the reliable and efficient operation of power systems.

It poses several challenges that need to be addressed effectively. Short circuit fault current in the DCDS reaches a high magnitude sharply after the arising of the fault because of the discharging capacitors [8]. Moreover, the absence of zero-crossing points in DC systems, makes fault detection more difficult compared to traditional AC networks [9]. Furthermore, the measurement sensors and devices deployed in the protection relay (PR) of the DCDS had a lot of noisy measured datasets which can cause maloperation of the PRs. Furthermore, the rapid evolution and integration of renewable energy sources in DCDS present additional challenges for fault detection. The varying characteristics of renewable energy sources, such as solar or wind power, can significantly affect the fault detection process [7]. Therefore, we need such a protection strategy that can detect all kinds of faults in DCDS under these challenging conditions without any maloperation and protection blinding.

Different kinds of protection methods for fault detection of DCDS were reported in previous literature. In [10] a rapid short circuit fault detection scheme was proposed for DC microgrids which incorporates fault classification and location. Authors in [11] proposed a fault detection method for DC microgrids involving electric vehicles (EV) and energy storage systems (ESS), employing dynamic mode decomposition and instantaneous frequency. This approach was tested in MATLAB 2019b on a single-bus DC microgrid and successfully detected various faults under noise distortions in measured signals. Similarly, in [12] authors proposed an empirical-mode decomposition (EMD) based fault detection method for the protection of DC microgrids with PV/EV/ESS systems. In [13] authors proposed a novel scheme based on Teager energy differences and resistance estimation to address the limitations in traditional fault detection for DC microgrids. Authors in [14] introduced a local current-based scheme for DC microgrid protection. This method enhances reliability by incorporating a central controller that serves as a backup in case of communication failures. A new protection method was proposed for DC microgrids [15], utilizing Shannon entropy to evaluate current waveform information for fault detection and classification. An improved composite strategy for DC microgrids was proposed in [16], addressing issues with communication-dependent protection and high-impedance short circuits. Reference [17] introduced a high-speed protection scheme for medium-voltage DCDS using MMA on energy signals, swiftly identifying, and classifying faults based on polarity detection. Similarly, a local current-based high impedance fault detection scheme was proposed in [18] for DC microgrid clusters using MMA, depicting fast and accurate fault detection without relying on communication channels. Reference [19] presented a differential current-based fault detection and location scheme for multiple Photovoltaic-based DC microgrids, addressing various fault types including pole-to-pole, pole-to-ground, and high resistive DC arc faults. A new traveling-wave-based method was proposed in [20], for rapid detection, classification, and location of different DC fault types in MVDC microgrids.

Some modern artificial intelligence (AI) and machine learning (ML) methods were also presented in previous literature. A novel method for resonant grounding DCDS was proposed in [21], utilizing continuous wavelet and convolutional neural networks for adaptive feature extraction and simultaneous fault detection. A data-driven fault detection and load monitoring solution for all-electric warships was presented in [22] using wavelet transform and computationally light machine learning, effectively identifying abnormal disturbances in load current profiles. In [23] a fault detection and isolation technique was proposed for DC microgrids using Wavelet transform and artificial neural networks, enabling fast and accurate fault detection without network de-energization. A fault detection and classification methodology for renewable microgrids was proposed in [24], utilizing the discrete wavelet transform and neural networks to enhance fault detection in nonlinear systems. In [25] an autoencoder neural networks-based protection scheme was developed to identify faults in DCDS. An online fault protection method was presented in [26] for low-voltage DC microgrids, leveraging a transfer learning-based convolution neural network, achieving 99.78% accuracy. In [27], a pseudo-data-driven method was proposed using analytical and model-based neural networks to localize both underdamped and over-damped faults without communication broadly. Previous works tried to address protection issues of the DCDS in depth but still have some limitations.

1. Fault detection methods may sometimes give false alarms, indicating a fault when there is none, or may fail to detect a fault when it is present.
2. Some fault detection methods may require complex algorithms or extensive calculations, making them difficult to implement.
3. Additionally, certain methods may only work effectively under specific conditions, limiting their applicability in different scenarios. Some fault detection methods rely on specific system parameters or models.
4. Changes in the system configuration, component characteristics, or load conditions can render these methods ineffective or inaccurate.

5. Implementing a few fault detection methods may involve significant costs, including the installation of monitoring equipment, data processing systems, and ongoing maintenance.
6. Some methods did not cater to noisy measurement conditions.

This research article presents a UHSFD scheme for DCDS utilizing two signal processing tools named the DMF and MMA. Initially, the DMF is applied to the noisy readings of the current signal acquired from the measurement unit of the relay. The DMF is used to estimate the true state of the current signal and reduce the measurement noise. In the second stage, the MMA computes a fault diagnosis criterion called DCR. This is the mathematical difference between the filtered output of MMA and the DMF's estimated current signal. The computed DCR variations are then compared with a pre-defined threshold setting to identify all the faults in the DCDS. The fault classification and section identification are done through the polarity of the computed MMABE. The proposed UHSFD scheme is tested on the DCDS test beds using MATLAB/Simulink 2022b software, the Windows 11 Home 64-bit Version: 22621.3155, and microprocessor 12th Gen Intel(R) Core (TM) i7-1255U. The results show that the suggested UHSFD scheme successfully identifies different types of DC faults quickly and accurately, without any false tripping or blinding. Several state-estimation algorithms have been utilized in previous research for fault detection which includes. Kalman filter [3], discrete Kalman filter [28], unscented Kalman filter [29], and some intelligent artificial learning and machine learning algorithms [30]. However, the most prominent and novel aspect of the proposed UHSFD method is that the utilized discrete median filter does not require difficult parameterization and tuning and has very low computational latency as compared to existing tools. The contribution of the proposed work includes.

1. Novel utilization of DMF & MMA in the time domain for fault diagnosis in DCDS.
2. Ultra High-speed fault diagnosis under 2.5 milliseconds with minimal computational burden.
3. Design of a simple fault diagnosis criterion independent of fault type and system conditions.
4. Autonomous handling of noisy sensor data by DMF and MMA to prevent false alarms.
5. Validation of the proposed UHSFD scheme up to a resistance of 300 ohms.
6. Low implementation cost without the need for high-cost devices like PMUs.

The arrangement of the remaining article is as follows. Section II focuses on the mathematical model and theoretical principles of the DMF and MMA algorithms, DCDS dynamics, and fault detection, classification, and location index computation. Section III depicts the methodology of the proposed UHSFD scheme step by step. Section IV presents the study test system of DCDS. The results and discussions of the proposed method are explained in section V. Finally, the paper is concluded with some future recommendations in section VI.

II. MATHEMATICAL MODEL OF THE PROPOSED UHSFD SCHEME

A. DYNAMICS OF THE DCDS

The proposed protection scheme is reliant on the DCR of the current signal. Therefore, this section focuses on defining the basic current signal model and its basic characteristics. In DCDS, the measured current signal exhibits dynamic behavior described by the fundamental relationship of Ohm's law, I=V/R, where I represents the measured current, V signifies the voltage across the system or component, and R stands for the resistance encountered by the current path. This equation encapsulates the intricate dynamics within DCDS. These dynamics manifest as transient spikes or drops in the measured current, influenced not only by the inherent characteristics of the distribution system such as line impedance and capacitance but also by external factors like noise, interference, and environmental conditions, thereby necessitating robust signal processing techniques for accurate interpretation and effective system management.

In the proposed UHSFD method, we exclusively employed the current signal to extract the necessary information for fault detection, classification, and localization. Therefore, the mathematical depiction of the current signal in DCDS is as follows.

$$I_n = e^{-\omega_1 t} i_k / W_1 L + \sin \omega_k + noise \tag{1}$$

The measured current I_n contains a lot of measurement and some arbitrary noise. Hence, should a fault arise at any segment of the DCDS, the fault current can be computed using Eq (1). Tanking the trigonometric derivative of Eq (1) results in an iterative discrete and nonlinear noisy state-space version of the measured current signal at the nth sample as follows.

$$I_n = e^{-\omega_1 t} i_n / W_1 L + \sin \omega_k + \varepsilon \tag{2}$$

where "ε" is the random error. However, the state space model of the current signal with the measurement equation is given as follows.

$$\widehat{Y_{(n)}} = h\left(x_{(n)}\right)\left(I_{(n)}\right) = P_{(n)} + A_{(n)} + I_{(n)} \tag{3}$$

And

$$X_{(n+1)} = \mathrm{F}(x_{(n)}) + \mathrm{g}(X_{(n)})(U_{(n)}) + W_n \tag{4}$$

where the $X_{(n+1)}$ is the estimated state, h is the measurement metrics, and $\widehat{Y_{(n)}}$ is the current measurement. With specific initial states and parameterization, the equations are employed by the DMF to process measured DC current signals within a DCDS.

B. DISCRETE MEDIAN FILTER

The rationale behind the use of a discrete median filter for fault diagnosis in DCDS lies in its ability to effectively remove impulse noise and spikes from the observed signals.

In DCDS, faults can occur due to various factors such as short circuits, ground faults, or insulation failures. These faults can result in sudden and transient changes in the voltage or current signals. When a fault occurs, it produces high-frequency components that appear as spikes or impulse noise in the system's signals. By definition, the DMF is a state estimation and noise reduction algorithm used to deal with non-linear and noisy sensor data.

They are mostly used as a location estimator, fault diagnosis, signal processing tools, noise reduction, and image processing tools. In the past, they have been used to generate smooth information and minimize noise. Additionally, they are less computationally challenging than other signal-processing algorithms. Although the DCDS also exhibits a non-linear feature while the DMF is a non-linear filter. As a result, in an extremely short period, the DMF generates the most auspicious feature estimation of electrical magnitudes from the set of non-linear and noisy sensor measurements. The step-by-step workflow of the discrete median filter algorithm is presented in FIGURE 1. While the pseudocode is presented in *TABLE 1*.

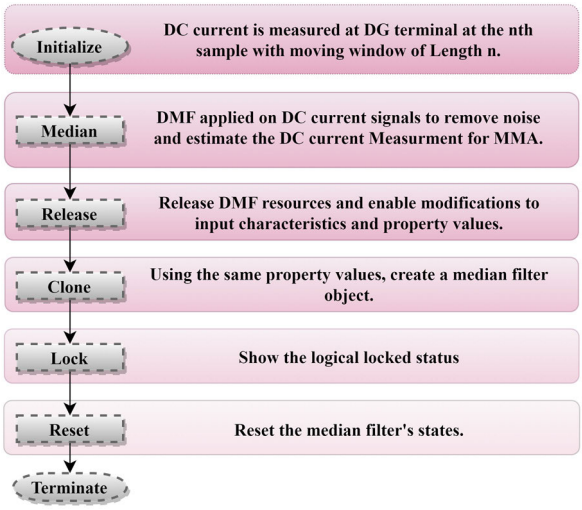

FIGURE 1. The Step-by-step depiction of the DMF algorithm.

The DMF computed the moving median using the sliding window method (SWM) as follows.

1. In this approach, the DMF generates the median from the data in a specified window that traverses over a particular channel on a current signal sample-to-sample for a defined length.
2. As a result, in SWM, each sample's results were the median of its latest sample and its (Len-1) prior samples, where Len is the window's length.
3. The procedure filled the window with zeros for dimension when the window did not yet contain enough data to compute the first Len1 outputs [2], [31], [32].
4. Finally, the estimated current signal using the DMF is presented as follows.

$$\widehat{I_n} = i_n + \mathrm{n} \tag{5}$$

TABLE 1. Pseudo code of DMF.

```
def median_filter (signal, window_size):
    filtered_signal = []
    half_window = window_size // 2

for i in range(len(signal)):

if i < half_window or i >= len(signal) -
half_window:
filtered_signal. append(signal[i])

else:

window = signal [i - half_window: i + half_window
+ 1]
median_value = sorted(window) [window_size // 2]
filtered_signal. append(median_value)

return filtered_signal.
```

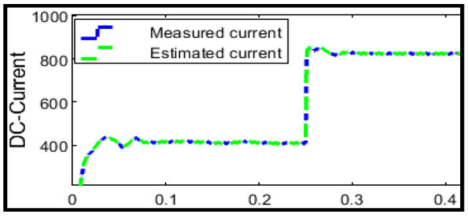

FIGURE 2. The measured and DMF-estimated DC-current signals.

where $\widehat{I_n}$ depict the estimated current with random noise n. FIGURE 2 shows the visual depiction of DMF-estimated current and measured current.

C. MATHEMATICAL MORPHOLOGY ALGORITHM

FIGURE 3 depicts the step-by-step workflow of MMA. Furthermore, the Pseudocode of MMA is depicted in *TABLE 2*. The utilization of mathematical morphology filters in fault diagnosis for DCDS is justified by their ability to capture and analyze signal variations, reduce noise, perform structural analysis, adapt to changing conditions, and provide fast and efficient processing. MMA, also known as morphological operators, are fundamental tools in this field used for tasks like noise reduction, edge detection, and image enhancement. There are two primary morphological operators: erosion and dilation depicted in FIGURE 4. These operators work with two key components: a structuring element (a small matrix or kernel) and an image, or signal. Applying mathematical morphology filters to an DMF's estimated current signal involves similar principles to working with images but in a one-dimensional signal domain [17], [18], [33], [34].

D. DCR CALCULATION USING MMA

Detecting faults in the DCDS presents unique challenges therefore, MMA plays a critical preprocessing step in the

TABLE 2. Pseudo code of MMA.

```
def erosion (signal, kernel_size):
    eroded_signal = []
    half_kernel = kernel_size // 2
    for i in range(len(signal)):
        if i < half_kernel or i >= len(signal) –
half_kernel:
            eroded_signal. append(signal[i])
        else:
            window = signal [i - half_kernel: i +
half_kernel + 1]
            min_value = min(window)
            eroded_signal. append(min_value)
return eroded_signal.
def dilation (signal, kernel_size):
    dilated signal = []
    half_kernel = kernel_size // 2
    for i in range(len(signal)):
        if i < half_kernel or i >= len(signal) –
half_kernel:
            dilated signal. append(signal[i])
        else:
            window = signal [i - half_kernel: i
half_kernel + 1]
            min_value = max(window)
            dilated signal. append(min_value)
    return dilated signal.
```

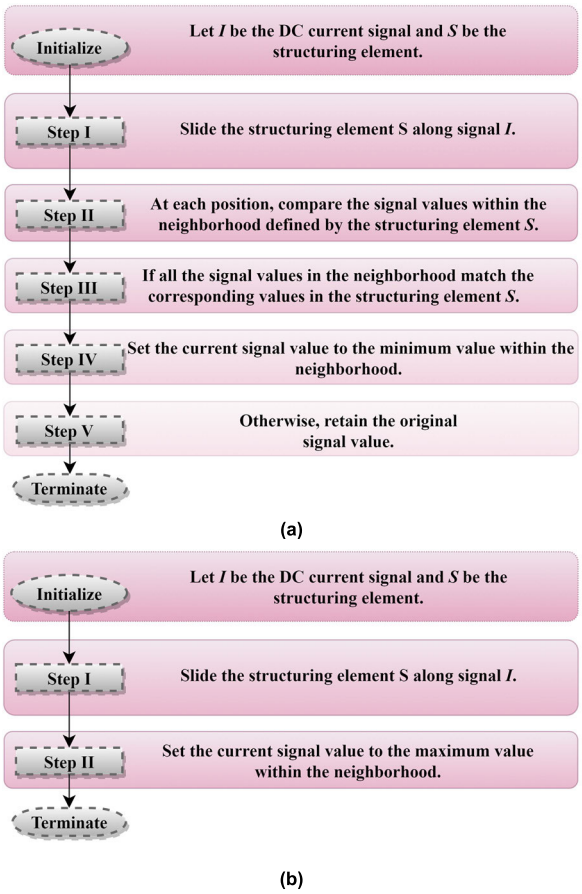

FIGURE 3. The Step-by-step depiction of the MMA algorithm (a) MMF Erosion Algorithm for Current Signal, (b) the MMF Dilation Algorithm for Current Signal.

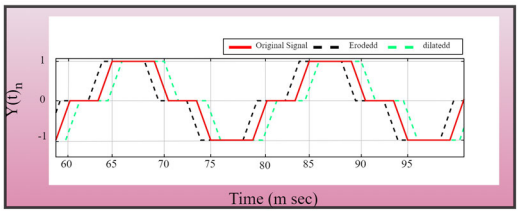

FIGURE 4. The original, eroded, and dilated Signature of MMA.

fault detection algorithms for the DCDS in the proposed UHSFD method. By enhancing signal quality, extracting relevant features, and enabling structural analysis, MMA significantly contributes to the accuracy and effectiveness of fault detection indices, ultimately enhancing the reliability and safety of DC distribution systems. MMA process of erosion, and dilation, the algorithm presented in the previous stage is utilized to compute residual from the estimated DCR using Eq (5). MMA can highlight areas in the signal that deviate significantly from the surrounding values, potentially indicating anomalies or unusual events in the current signal. Adjusting the structuring element size and performing additional processing can refine the identification of relevant deviations in the signal. The DCR signature obtained represents areas where significant deviations occurred compared to the surrounding values. The mathematical steps involved in calculating current residuals using an MMA algorithm are as follows.

Step 1: Signal Preprocessing

Start with a discrete current signal $\widehat{I_n} = [\widehat{I_1} + \widehat{I_2} + \widehat{I_3} \ldots\ldots \widehat{I_k}]$, where $\widehat{I_k}$ represents the value of the estimated signal at time k. Choose a structuring element S with a specific size and shape. It could be a simple window or kernel for local operations.

Step 2: Erosion Operation

The erosion operation E on the signal $\widehat{I_k}$ with the structuring element S is represented as

$$\mathrm{E}(I_k, \mathrm{S}) \tag{6}$$

For each I_k from 1 to k, calculate the eroded signa $I_{k_{eroded}}$ as:

$$\mathrm{I}_{\mathrm{k}_{\mathrm{eroded}}}[\mathrm{k}] = \mathrm{min}_{\mathrm{j}\epsilon \mathrm{S}}(\mathrm{I}[\mathrm{k}+\mathrm{j}]) \tag{7}$$

Here, j iterates over the indices within the structuring element S and finds the minimum value in the neighborhood of each I_k within the signal I.

Step 3: Dilation Operation

The dilation operation D on the eroded signal $I_{k_{eroded}}$ with the same structuring element S is represented as.

$$\mathrm{D}(I_{k_{eroded}}, \mathrm{S}) \tag{8}$$

For each I_k from 1 to k, calculate the dilated signal $I_{k_{dilated}}$ as:

$$\mathrm{I}_{\mathrm{k_{dilated}}}[\mathrm{k}] = \min_{\mathrm{j}\in \mathrm{S}}(\mathrm{I}_{\mathrm{k_{eroded}}}[\mathrm{k}+\mathrm{j}]) \tag{9}$$

Here, j iterates over the indices within the structuring element S and finds the maximum value in the neighborhood of each eroded $I_{k_{eroded}}[k]$.

Step 4: Calculate Residuals

Subtract the dilated signal $I_{k_{dilated}}[k]$ from the original signal $\widehat{I_n}$ to obtain the current residuals also stated as DCR.

$$DCR_k = \widehat{I_n} - I_{k_{dilated}}[k] \tag{10}$$

DCR_k indicates the estimated DC residuals at kth sample. This produces a signal where deviations or anomalies from the local maxima within the structuring element are highlighted as residual values. These steps outline the mathematical operations involved in computing DCR using mathematical morphology filters. The erosion and dilation operations manipulate the signal based on the structuring element to isolate and extract deviations in the original signal, leading to the computation of the residuals. Adjusting the structuring element size and type can impact the sensitivity of anomaly detection in the signal.

E. MMABE CALCULATION USING MMA

In the context of mathematical morphology applied to current signals, the concept of "energy" might differ from traditional signal processing applications. Morphological operations, when applied to signals like currents, might involve analyzing and extracting features.

A time series f current values represented by $\widehat{I_n(t)}$, where t denotes time. Then, apply morphological operations like erosion and dilation to extract features from the current signal. For instance, if the extracted features represent variations or anomalies in the current, you might calculate the sum of squared feature values:

$$MMABE_n = \sum \widehat{I_n}(dilate + eroded\ nonfundamental\ features) \tag{11}$$

where, Feature "t" represents the value of the extracted feature at time. It is observed by detailed simulations that the MMABE exhibits different polarity during different faults. the MMABE during the pole-to-pole fault is.

$$\left\{ \begin{array}{l} MMABE_n\ is\ negative\ on\ one\ while \\ zero\ on\ other\ end. \end{array} \right\} = pole\ to\ pole\ fault \tag{12}$$

And the MMABE during the positive pole to ground fault is.

$$\left\{ \begin{array}{l} MMABE_n\ is\ opposite\ on\ both \\ ends. \end{array} \right\} = positive\ pole\ to\ ground\ fault \tag{13}$$

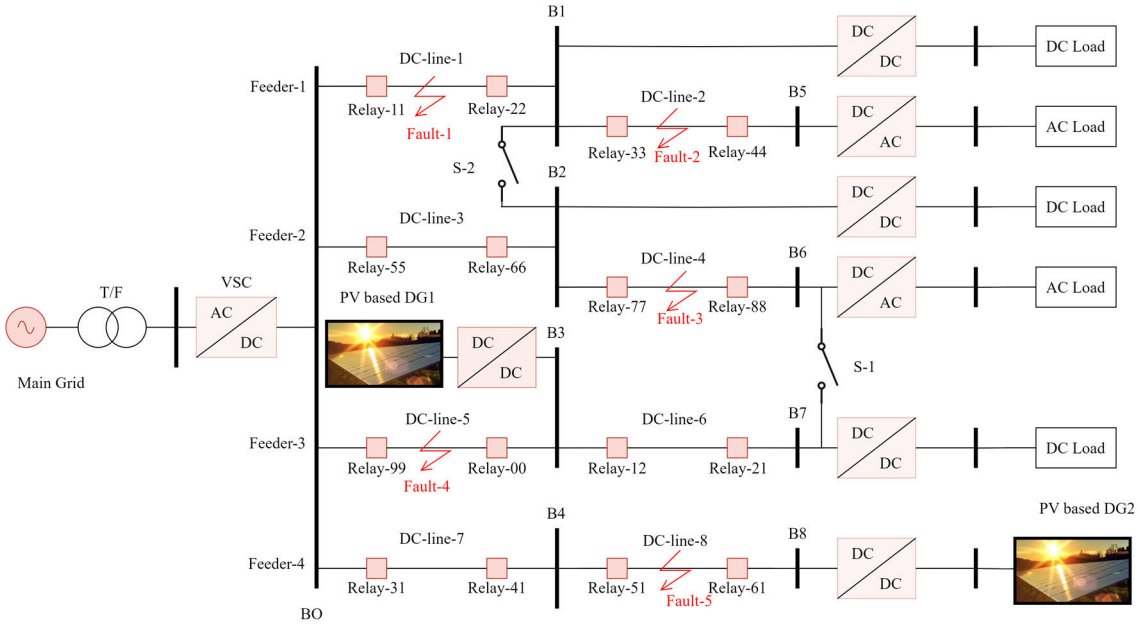

FIGURE 5. The DCDS study test bed for detailed DC fault analysis.

While during negative pole to ground faults the MMABE is depicted as follows.

$$\left\{ \begin{array}{l} MMABE_n \text{ is negative on} \\ \text{both end}. \end{array} \right\} = \text{negative pole to ground fault} \quad (14)$$

Hence, the polarity in Eqs 12, 13 and 14 are utilized for the decision of fault classification and localization.

F. THRESHOLD SETTING

An accurate and precise threshold setting is necessary for any scheme to avoid malfunctioning relays. For that purpose, the proposed scheme has been tested for different worst simulation conditions. The maximum and minimum operation conditions are cross-checked for the estimation of correct values. It is observed that the ideal value of DCR for no fault condition is noted as 0 but a practically little bit more than zero, therefore, the threshold is on the safe side chosen as 5 absolute values, because we had a very huge margin to choose from the threshold value. The proposed scheme has been tested for different fault conditions like pole-to-pole (P-P) and positive pole-to-ground (PP-G) faults on these threshold settings. Hence the scheme operated successfully under all regimes.

III. STUDY DCDS-TEST SYSTEMS

The DCDS test bed engaged for validation and extensive performance analysis of the proposed UHSFD scheme have been modeled in MATLAB/Simulink software. The single-line diagram of the study test bed is depicted in FIGURE 5. Different fault locations are depicted in the figure on distribution line segments. It consists of four feeders and is further segregated into nine buses from B 0 to B 8. In addition, the whole DCDS is connected to a utility grid via IGBT-based three-level VSC. The VSC maintained the voltage level of both study DCDS test beds at ± 2.5Kv. Two PV-based DGs are also feeding the DCDS penetrated at B0 and B3 respectively. Two switches, S 1 between B6 and B7 while S 2 between B1 and B2 are used for test system configurational changes like radial, loop and meshed. Each PV-based DG unit is comprised of 2MW power capacity. The data set of DC distribution set used in the proposed method is generated through an extensive and comprehensive simulation under various operation conditions, locations, different buses, and various fault impedance values [20], [31].

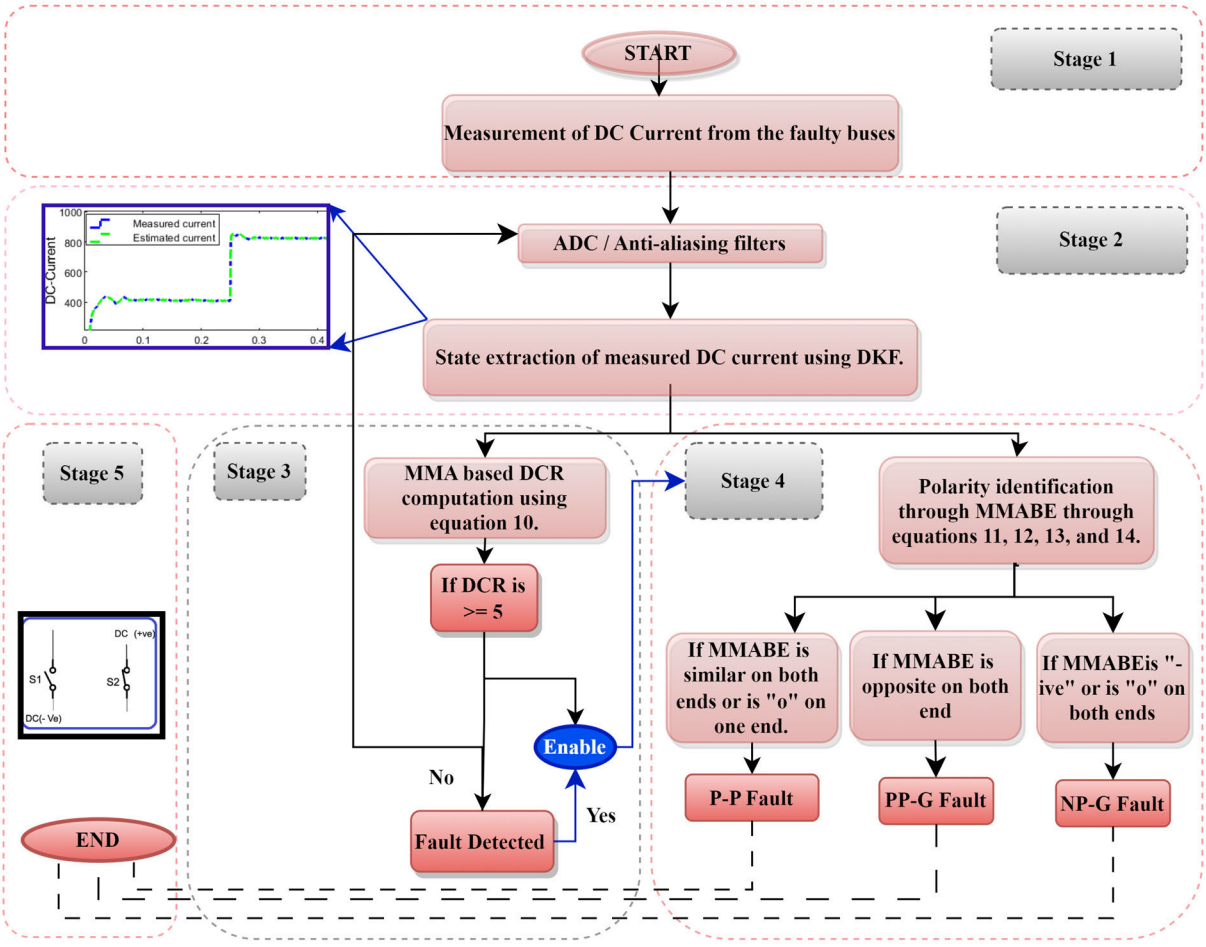

FIGURE 6. The schematic diagram the proposed UHSFD method.

IV. METHODOLOGY OF PROPOSED UHSFD SCHEME

A structured methodology, termed UHSFD, has been developed specifically for fault detection in DC distribution systems (DCDS). This method is meticulously organized into five clear sections represented in FIGURE 6.

The process begins with the acquisition of the current signal from the measurement unit embedded within protective relays. These signals, however, exist in an analog format initially and undergo transformation through an Analog-to-Digital Converter (ADC) with a sampling frequency of 1600 Hz, converting them into a digital form. It is imperative to note that the ADC plays a pivotal role in capturing and processing not just ordinary signals but specifically targets anomalous, highly fluctuating readings that might signify potential faults or disturbances within the system. Moreover, the antialiasing of the current signal is done using a Bezel filter with a cut-off frequency of 3.5 kHz.

In the second stage, following the conversion into discrete signals, these current signals undergo preprocessing facilitated by the DMF. The role of DMF encompasses two pivotal steps aimed at enhancing the quality of the acquired discrete current signals. 1st, using the DMF framework, a state estimation process is initiated on the discrete current signal. 2nd, the DMF focuses its operations on the refining the signal by employing noise reduction process, ensuring a clearer, more refined representation that minimizes unwanted distortions or interferences present within the signal during measurement or any random noise.

In third stage, Upon the completion of state estimation and noise reduction within the DMF, the refined and estimated signal is directed towards a specialized filtering mechanism known as the Mathematical Morphology Filter. The primary objective of the MMA is to scrutinize the estimated signal, seeking out deviations that might signify potential faults or disturbances within the DCDS. Leveraging mathematical operations rooted in morphological analysis, the MMA computes DCR using Eq 10, which serve as fault detection index. These computed DCR serve as pivotal indicators, providing a clearer delineation between normal system behaviour and potential fault conditions, thereby enhancing the fault identification capabilities of the DCDS. Secondly, the MMABE is computed for fault classification and section identification using Eq 11.

Fourth stage involves a comparison of the computed DCR within the PR against predefined threshold values. This comparison serves as a critical checkpoint, evaluating the magnitude of deviation from normal behaviour. If the observed variations exceed the pre-specified threshold values, indicating a fault condition and the protective relay triggers an isolation logic.

Finally, this activation results in the generation of a trip signal, a vital safety mechanism designed to isolate the identified

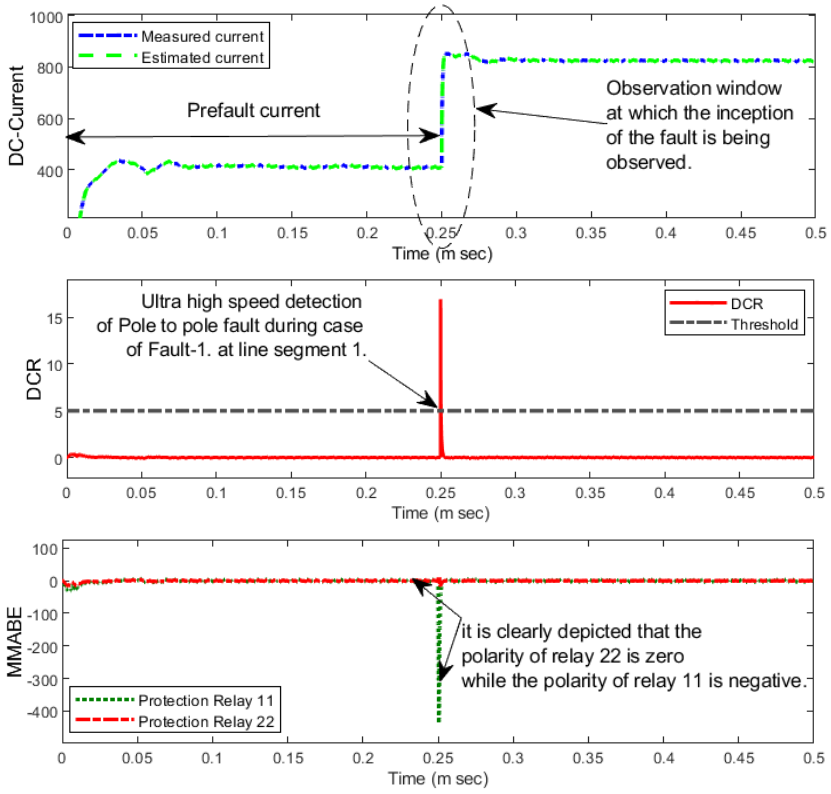

FIGURE 7. The DC current signature, DCR signature, and MMABE signature during P-P fault at DC line segment 1.

faulty section from the rest of the system promptly. This swift disengagement of the faulty segment ensures the preservation of the overall system integrity, preventing potential cascading effects that could jeopardize the entire system's operation and safety.

V. RESULTS AND DISCUSSION

On the DCDS test beds, numerous simulations have been run to assess the robustness of the proposed UHSFD scheme. Different fault conditions were simulated for the DC faults under various system conditions. The PP-G, NP-G, and P-P faults are addressed in this study. Moreover, several case studies were also carried out with different parameters to authorize the robustness of the proposed UHSFD scheme with varying fault resistance and location.

A. POLE-TO-POLE FAULTS

This subsection illustrates the detailed testing of the proposed scheme during P-P faults. Therefore, multiple such faults are tested on various locations of the DCDS test bed as depicted in TABLE 3. But due to lack of space and ease of readers understanding, few cases are elaborated on here for the validation of the proposed UHSFD scheme.

TABLE 3. Various faults cases on DCDS test bed.

Faulty section	Noise level (db.)	Network configuration	Fault types	Fault location	DCR (peak)	MMABE (polarity)
DC line 1	5	Radial	PP-G	25 km to B0	35	+ive PR 11 while -ive at PR 22
DC line 2	9	Looped	NP-G	64 km to B1	55	-ive PR 33 while -ive at PR 44
DC line 3	4	Radial	P-P	66 km to B0	33	-ive PR 55 while zero at PR 66
DC line 4	10	Meshed	PP-G	33 km to B2	56	+ive PR 77 while -ive at PR 88
DC line 5	8	Looped	NP-G	12 km to B0	32	-ive PR 99 while -ive at PR 00
DC line 6	12	Meshed	P-P	43 km to B3	22	-ive PR 12 while zero at PR 21
DC line 7	15	Radial	NP-G	10 km to B0	52	-ive PR 31 while -ive at PR 41
DC line 8	14	Radial	PP-G	24 km to B4	65	+ive PR 51 while -ive at PR 61

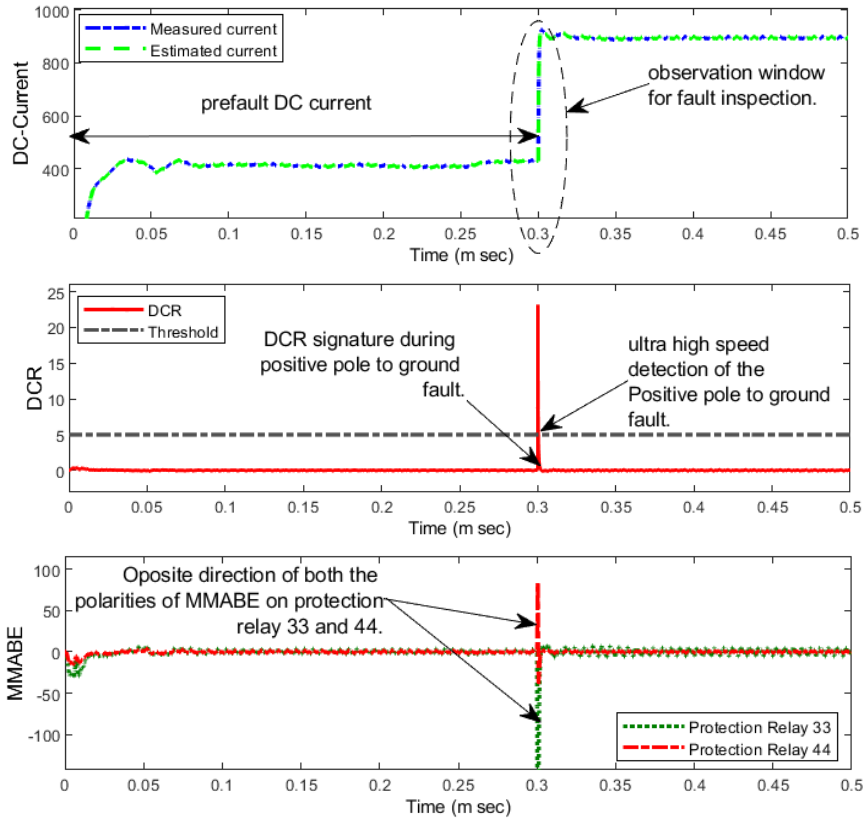

FIGURE 8. The DC current signature, DCR signature, and MMABE signature during PP-G fault at DC line segment 2.

A P-P fault was initiated on the DC line segment 1 at the time instant of 0.25 m sec, 20 km away from the B0. The DC-current signature and DCR signatures during this fault are depicted in FIGURE 7. The results show that after the occurrence of a fault, the corresponding relay 11 instantly detects the fault in less than 2.5 m sec successfully. However, the polarity of PR 11 is negative, and PR 22 is zero which indicates the presence of P-P fault in the DC line segment 1.

B. POSITIVE POLE-TO-GROUND FAULTS

This subsection illustrates the detailed testing of the proposed UHSFD scheme during PP-G faults. Therefore, multiple such faults are tested on various locations of the DCDS testbed as illustrated in TABLE 3. However, due to lack of space and ease of readers' understanding, few cases are elaborated on here for the validation of the proposed UHSFD scheme.

A PP-G fault occurred on the DC line segment 2 at the time instant of 0.3 m sec, 50 km away from the B1. The DC-current

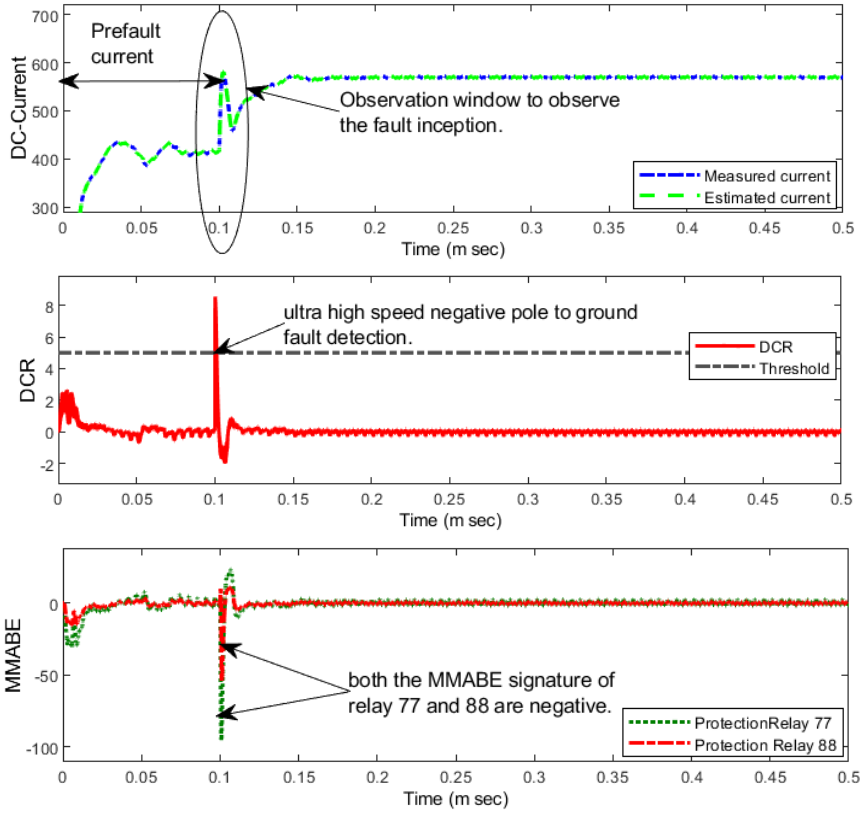

FIGURE 9. The DC current signature, DCR signature, and MMABE signature during NP-G fault at DC line segment 4.

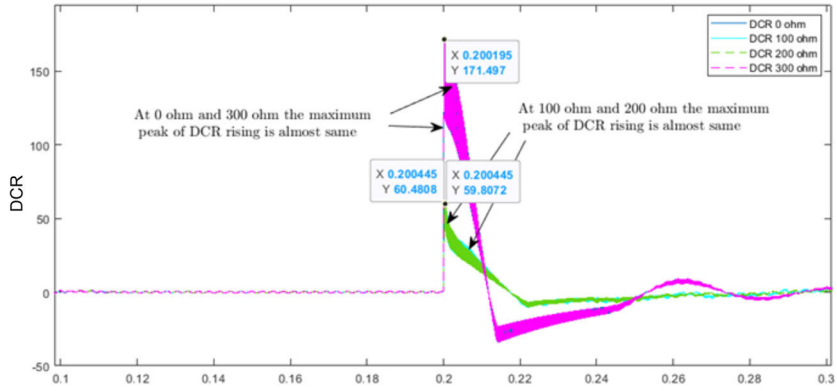

FIGURE 10. The DCR signature at DC line segment 8 during different resistances.

and DCR signatures at 33 during this fault are depicted in FIGURE 8. The results indicate that after the occurrence of a fault, the corresponding relay 33 instantly detects the fault in less than 2.5 m sec successfully. However, the opposite polarity of PR 33, and PR 44 indicates the presence of PP-P fault in DC line segment 2.

C. NEGATIVE POLE-TO-GROUND FAULTS

This subsection illustrates the detailed testing of the proposed UHSFD scheme during NP-G faults. Therefore, multiple such faults are tested on various locations of the DCDS testbed as illustrated in TABLE 3. However, due to lack of space and ease of readers understanding, few cases are elaborated on here for the validation of the proposed UHSFD scheme.

An NP-G fault occurred on the DC line segment 4 at the time instant of 0.1m sec, 20 km away from the B2. The DC-current and DCR signatures at PR 77 during this fault are depicted in FIGURE 9. The results indicate that after the occurrence of a fault, the corresponding PR 77 instantly detects the fault in less than 2.5 m sec. However, the polarity is negative, on both the PR 77 and PR 88 which indicates the presence of NP-P fault in the DC line segment 4.

D. RESULTS DURING VARYING RESISTANCE FAULTS

This section illustrates the detailed testing of the proposed UHSFD scheme during the various values of fault resistance. Therefore, multiple P-P and P-G faults are tested on several locations with different values of resistances. However, due to a lack of space and ease of readers' understanding, one case is elaborated on here for the validation of the proposed UHSFD scheme.

A P-P fault occurred at the DC line segment 8 at the time instant of 0.2 m sec, 65 km away from the B4 with the fault resistance of 0, 100, 200, and 300 0hm. The DCR signatures at relay 51 during this fault are depicted in FIGURE 10. The results indicate that after the occurrence of a fault, the corresponding relay 51 instantly detects the fault in less than 2.5 m sec successfully for all values of the resistances.

E. DIFFERENT GRID CONFIGURATIONAL CHANGES RESULTS

This section illustrates the detailed testing of the proposed UHSFD scheme during the various configurational changes like radial, loop, and meshed network. Therefore, multiple P-P and P-G faults are tested with several configurational changes. However, due to a lack of space and ease of readers' understanding, one case is elaborated on here as proof, while some cases were also mentioned in TABLE 3.

A NP-G fault occurred at the DC line segment 3 at the time instant of 0.45 m sec, 15 km away from the B0 with loop configuration when S1 is open and S2 is close. Moreover, the PV-based DG 1 is out of operation during the simulation of this case to check the DG's intermittency. The DCR signature at relay 55 during this fault is depicted in FIGURE 11.

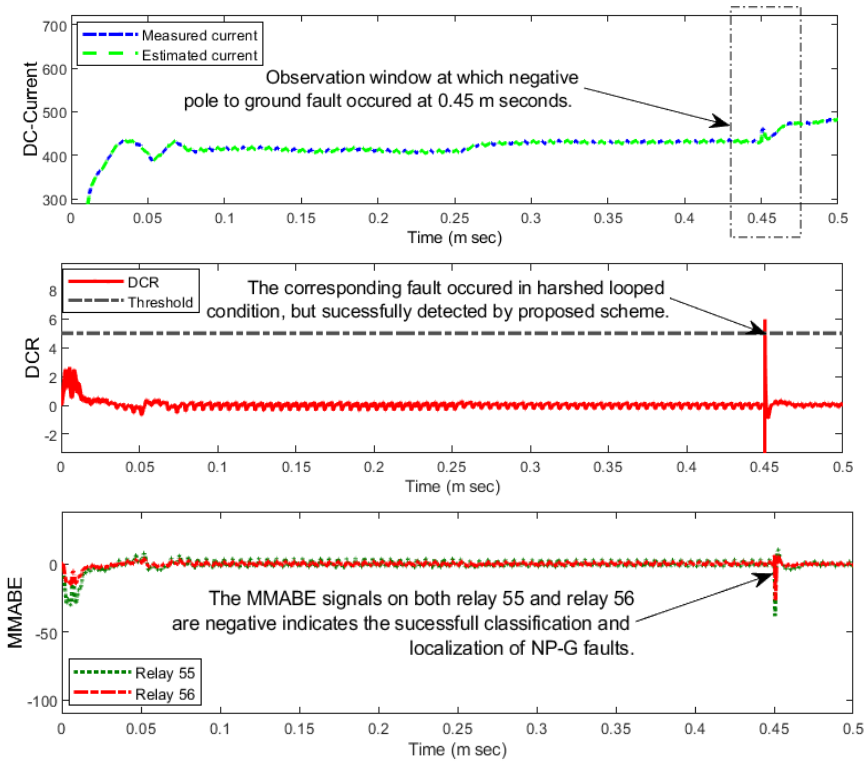

FIGURE 11. The DC current signature, DCR signature, and MMABE signature during NP-G fault at DC line segment 3 when PV-based DG 1 is out to check DG's intermittency and looped configuration.

The results indicate that after the occurrence of a fault, the corresponding relay 55 instantly detects the fault in less than 2.5 m sec successfully.

F. NOISY MEASUREMENT CONDITIONS RESULTS

This section illustrates the detailed testing of the proposed UHSFD scheme during the various noise measurement conditions as depicted in TABLE 3. Therefore, multiple P-P and P-G faults are tested on several locations with different values of resistances based on noisy measurement conditions. However, due to a lack of space and ease of readers' understanding, one case is elaborated on here for the validation of the proposed UHSFD scheme.

A P-P fault occurred at the DC line segment 6 at the time instant of 0.022 m sec, 17 km away from the B3 with meshed configuration when both S1 and S2 are close. Moreover, this

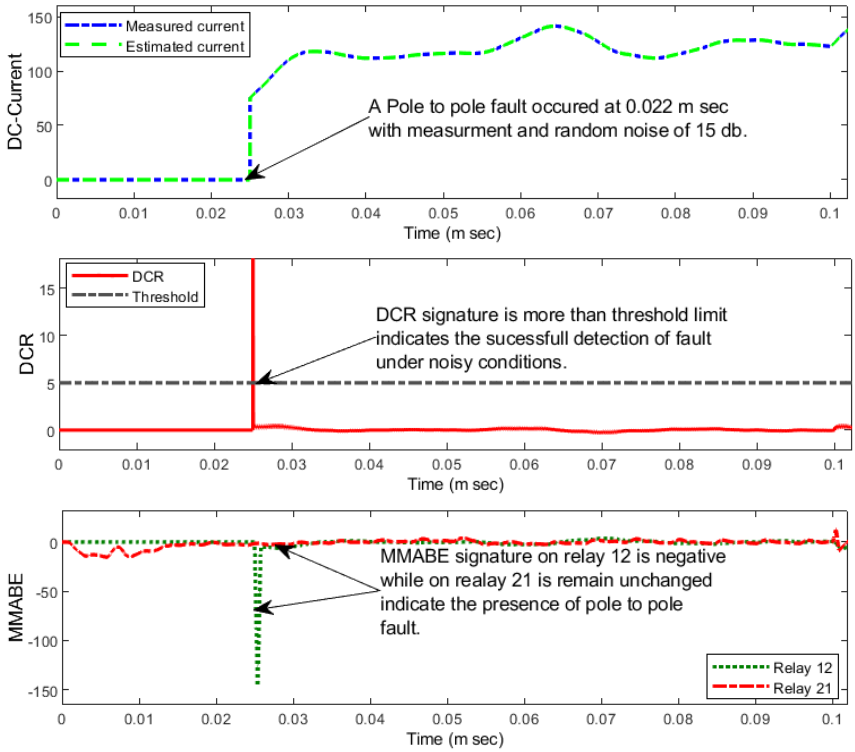

FIGURE 12. The DC current signature, DCR signature, and MMABE signature during P-P fault at DC line segment 6.

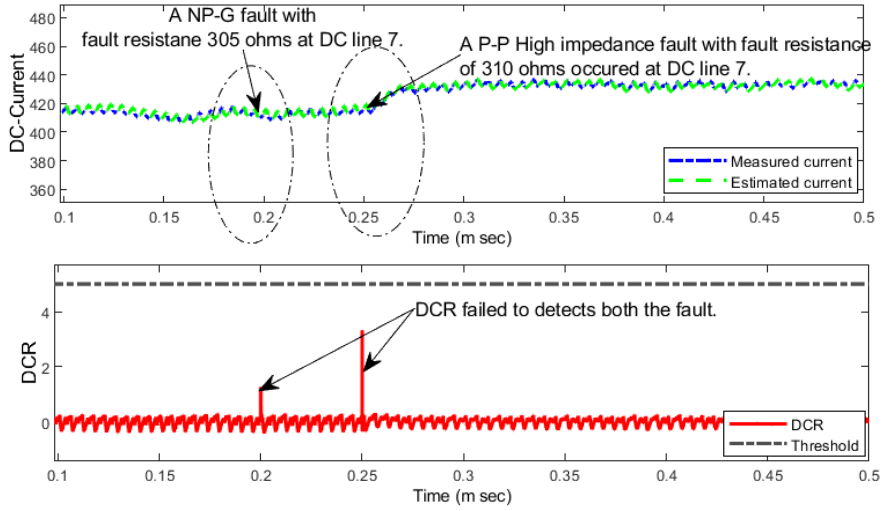

FIGURE 13. The DC current signature and DCR signature during a NP-G and P-P fault at DC line segment 7.

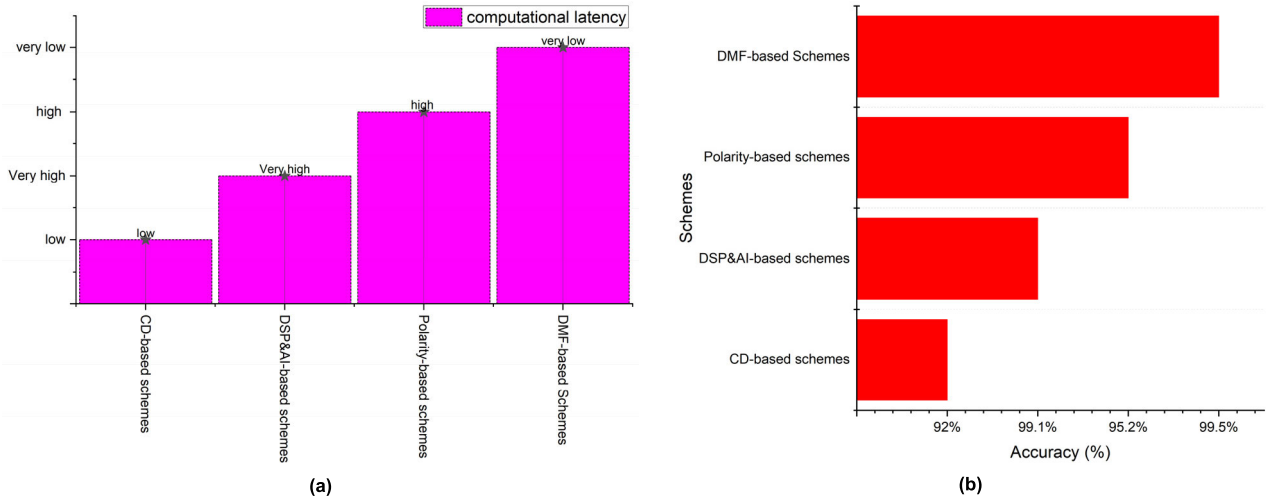

FIGURE 14. The (a) Computational latency and (b) Accuracy.

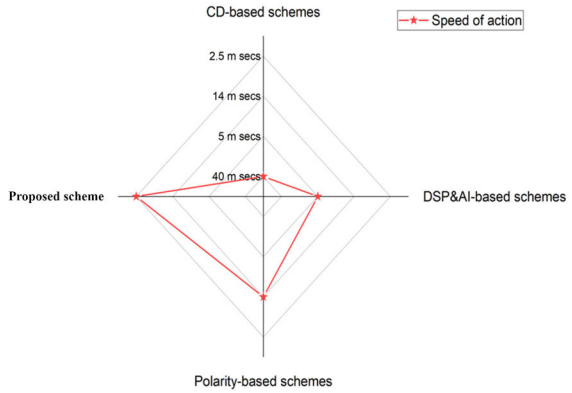

FIGURE 15. The radar chart of Speed of action.

fault is tested with the gaussian random noise of 5 db. Besides that, the DCR signature at relay 12 during this fault is depicted in FIGURE 12. The results indicate that after the occurrence of a fault, the corresponding relay 12 instantly detects the fault in less than 2.5 m sec successfully.

G. PROPOSED UHSFD SCHEME FAILURE CONDITIONS RESULTS

This section illustrates the detailed testing of the proposed UHSFD scheme during the various false failure conditions as depicted in FIGURE 13. It is depicted that an NP-G fault occurred at 0.2 m sec with fault resistance of 305 ohms; the scheme fails to detect this high impedance fault. Similarly, another P-P fault was simulated at 0.25 m seconds with fault resistance of 310 ohms; the scheme fails to detect this high impedance fault.

VI. COMPARATIVE ANLYSIS

This subsection mainly focuses on the accuracy, computational burden, and speed of action of the proposed method with some other existing schemes like polarity-based methods, AI&DSP-based methods, and current derivative (CD)-based methods [2], [3], [14], [15], [16], [17], [18], [19], [20], [21], [22], [23], [24], [25], [26], [27], [28], [29], [30] as depicted in *TABLE 4*. Firstly, the computational latency comparison of the presented method is shown in FIGURE 14 (a). Secondly, a lot of case studies were performed, and the overall accuracy has been calculated as depicted in FIGURE 14 (b), while accuracy is computed as.

TABLE 4. Comparative analysis of PF with existing methods.

Parameters	Existing methods			The UHSFD method
	Polarity based methods	CD-based methods	AI&DSP-based methods	
Noise consideration	×	✓	×	✓
Security	✓	×	×	✓
Threshold adjustment	×	✓	×	×
Signal processing tool	×	Better	Good	Excellent
Implication	Complex	Simple	Complex	Simple
Sensitivity	Moderate	Low	High	High

$$Accuracy = \frac{sucessful\ operations}{total\ performed\ operation} \tag{15}$$

The third parameter used for the performance analysis of the proposed scheme is the speed of action. The results in the radar chart shown in FIGURE 15 indicate that the proposed scheme shows better performance as compared to existing schemes. conclusively, the suggested technique operates quickly and is easy to apply. The proposed scheme is superior to most of the previous benchmark schemes in some aspects.

VII. CONCLUSION

The proposed Ultra High-speed Fault Diagnosis scheme using a Discrete Median Filter and Mathematical Morphology Algorithm proved to be effective in fault diagnosis for DCDS. The DMF preprocessing stage successfully estimated the state and reduced noise in the acquired current. The UHSFD Scheme computed the DCR using the MMFA on the DMF-estimated current signal, allowing for the detection of faults by crossmatching variations in the computed DCR with pre-defined threshold settings. Then, the Mathematical Morphology algorithm-based Energy computed in the third stage facilitated fault classification and section identification. The results indicate that the proposed scheme has very low computational latency, having 99.5 % accuracy, operation time less than 2.5 m sec, and capable of detecting DC faults in radial, looped, and meshed topology. Furthermore, the hardware implementation of the proposed scheme is aimed at future work.

REFERENCES

[1] K. Kant and O. H. Gupta, "DC microgrid: A comprehensive review on protection challenges and schemes," *IETE Tech. Rev.*, vol. 40, no. 4, pp. 574–590, Jul. 2023, doi: 10.1080/02564602.2022.2136271.

[2] F. Mumtaz, K. Imran, A. Abusorrah, and S. B. A. Bukhari, "Harmonic content-based protection method for microgrids via 1-dimensional recursive median filtering algorithm," *Sustainability*, vol. 15, no. 1, p. 164, Dec. 2022, doi: 10.3390/su15010164.

[3] F. Mumtaz, K. Imran, S. B. A. Bukhari, K. K. Mehmood, A. Abusorrah, M. A. Shah, and S. A. A. Kazmi, "A Kalman filter-based protection strategy for microgrids," *IEEE Access*, vol. 10, pp. 73243–73256, 2022, doi: 10.1109/ACCESS.2022.3190078.

[4] M. S. Alam, F. S. Al-Ismail, S. M. Rahman, M. Shafiullah, and M. A. Hossain, "Planning and protection of DC microgrid: A critical review on recent developments," *Eng. Sci. Technol., Int. J.*, vol. 41, May 2023, Art. no. 101404, doi: 10.1016/j.jestch.2023.101404.

[5] M. Mishra, B. Patnaik, M. Biswal, S. Hasan, and R. C. Bansal, "A systematic review on DC-microgrid protection and grounding techniques: Issues, challenges and future perspective," *Appl. Energy*, vol. 313, May 2022, Art. no. 118810, doi: 10.1016/j.apenergy.2022.118810.

[6] S. Mohanty, A. Bhanja, S. P. Gautam, D. Chittathuru, S. K. Dash, M. Mangaraj, R. Chinthaginjala, and A. M. Alamri, "Review of a comprehensive analysis of planning, functionality, control, and protection for direct current microgrids," *Sustainability*, vol. 15, no. 21, p. 15405, Oct. 2023, doi: 10.3390/su152115405.

[7] L. Tang, Y. Han, A. S. Zalhaf, S. Zhou, P. Yang, C. Wang, and T. Huang, "Resilience enhancement of active distribution networks under extreme disaster scenarios: A comprehensive overview of fault location strategies," *Renew. Sustain. Energy Rev.*, vol. 189, Jan. 01, 2024, Art. no. 113898, doi: 10.1016/j.rser.2023.113898.

[8] M. Y. Arafat, M. J. Hossain, and M. M. Alam, "Machine learning scopes on microgrid predictive maintenance: Potential frameworks, challenges, and prospects," *Renew. Sustain. Energy Rev.*, vol. 190, Feb. 2024, Art. no. 114088, doi: 10.1016/j.rser.2023.114088.

[9] S. A. Hosseini, B. Taheri, S. H. H. Sadeghi, and A. Nasiri, "An overview of DC microgrid protection schemes and the factors involved," *Electr. Power Compon. Syst.*, pp. 1–31, Sep. 2023, doi: 10.1080/15325008.2023.2251469.

[10] Q. Wan, S. Zheng, and C. Shi, "A rapid diagnosis technology of short circuit fault in DC microgrid," *Int. J. Electr. Power Energy Syst.*, vol. 147, May 2023, Art. no. 108878, doi: 10.1016/j.ijepes.2022.108878.

[11] A. Sistani, S. A. Hosseini, V. S. Sadeghi, and B. Taheri, "Fault detection in a single-bus DC microgrid connected to EV/PV systems and hybrid energy storage using the DMD-IF method," *Sustainability*, vol. 15, no. 23, p. 16269, Nov. 2023, doi: 10.3390/su152316269.

[12] B. Taheri and A. Shahhoseini, "Direct current (DC) microgrid control in the presence of electrical vehicle/photovoltaic (EV/PV) systems and hybrid energy storage systems: A case study of grounding and protection issue," *IET Gener., Transmiss. Distrib.*, vol. 17, no. 13, pp. 3084–3099, Jul. 2023, doi: 10.1049/gtd2.12882.

[13] G. K. Rao and P. Jena, "A novel fault identification and localization scheme for bipolar DC microgrid," *IEEE Trans. Ind. Informat.*, vol. 19, no. 12, pp. 11752–11764, Dec. 2023, doi: 10.1109/TII.2023.3252409.

[14] N. R. Nareddy, R. Pitchaimuthu, and M. Sridharan, "Current index based protection technique for low voltage DC microgrid," *Electr. Power Syst. Res.*, vol. 220, Jul. 2023, Art. no. 109360, doi: 10.1016/j.epsr.2023.109360.

[15] R. Rahmani, S. H. H. Sadeghi, H. Askarian-Abyaneh, and M. J. Emadi, "An entropy-based scheme for protection of DC microgrids," *Electr. Power Syst. Res.*, vol. 228, Mar. 2024, Art. no. 110010, doi: 10.1016/j.epsr.2023.110010.

[16] W. Zhang, H. Zhang, and N. Zhi, "A novel protection strategy for DC microgrid considering communication failure," *Energy Rep.*, vol. 9, pp. 2035–2044, Sep. 2023, doi: 10.1016/j.egyr.2023.04.186.

[17] M. A. Shah, S. B. A. Bukhari, K. Imran, K. K. Mehmood, F. Mumtaz, A. Abusorrah, S. A. A. Kazmi, and A. Wadood, "High speed protection of medium voltage DC distribution system using modified mathematical morphology," *IET Renew. Power Gener.*, vol. 16, no. 14, pp. 3134–3148, Oct. 2022, doi: 10.1049/rpg2.12564.

[18] N. Bayati, H. R. Baghaee, A. Hajizadeh, M. Soltani, and Z. Lin, "Mathematical morphology-based local fault detection in DC microgrid clusters," *Electr. Power Syst. Res.*, vol. 192, Mar. 2021, Art. no. 106981, doi: 10.1016/j.epsr.2020.106981.

[19] S. Dhar, R. K. Patnaik, and P. K. Dash, "Fault detection and location of photovoltaic based DC microgrid using differential protection strategy," *IEEE Trans. Smart Grid*, vol. 9, no. 5, pp. 4303–4312, Sep. 2018, doi: 10.1109/TSG.2017.2654267.

[20] K. A. Saleh, A. Hooshyar, and E. F. El-Saadany, "Ultra-high-speed traveling-wave-based protection scheme for medium-voltage DC microgrids," *IEEE Trans. Smart Grid*, vol. 10, no. 2, pp. 1440–1451, Mar. 2019, doi: 10.1109/TSG.2017.2767552.

[21] M.-F. Guo, X.-D. Zeng, D.-Y. Chen, and N.-C. Yang, "Deep-Learning-Based Earth fault detection using continuous wavelet transform and convolutional neural network in resonant grounding distribution systems," *IEEE Sensors J.*, vol. 18, no. 3, pp. 1291–1300, Feb. 2018, doi: 10.1109/JSEN.2017.2776238.

[22] Y. Ma, A. Maqsood, D. Oslebo, and K. Corzine, "Wavelet transform data-driven machine learning-based real-time fault detection for naval DC pulsating loads," *IEEE Trans. Transp. Electrific.*, vol. 8, no. 2, pp. 1956–1965, Jun. 2022, doi: 10.1109/TTE.2021.3130044.

[23] D. K. J. S. Jayamaha, N. W. A. Lidula, and A. D. Rajapakse, "Wavelet-multi resolution analysis based ANN architecture for fault detection and localization in DC microgrids," *IEEE Access*, vol. 7, pp. 145371–145384, 2019, doi: 10.1109/ACCESS.2019.2945397.

[24] A. Cano, P. Arévalo, D. Benavides, and F. Jurado, "Integrating discrete wavelet transform with neural networks and machine learning for fault detection in microgrids," *Int. J. Electr. Power Energy Syst.*, vol. 155, Jan. 2024, Art. no. 109616, doi: 10.1016/j.ijepes.2023.109616.

[25] T. Tabassum, O. Toker, and M. R. Khalghani, "Cyber–physical anomaly detection for inverter-based microgrid using autoencoder neural network," *Appl. Energy*, vol. 355, Feb. 2024, Art. no. 122283, doi: 10.1016/j.apenergy.2023.122283.

[26] S. Veerapandiyan and V. Sugavanam, "On-line fault identification, location, and seamless service restoration using transfer learning-based convolution neural network for low-voltage DC microgrid," *Electric Power Compon. Syst.*, vol. 51, no. 8, pp. 785–808, May 2023, doi: 10.1080/15325008.2023.2183997.

[27] W. Javed, D. Chen, and I. Kucukdemiral, "Fault identifiability and pseudo-data-driven fault localization in a DC microgrid," *Int. J. Electr. Power Energy Syst.*, vol. 148, Jun. 2023, Art. no. 108944, doi: 10.1016/j.ijepes.2023.108944.

[28] F. Mumtaz, K. Imran, H. Rehman, and H. Ali Qureshi, "Hardware supported fault detection and localization method for AC microgrids using mathematical morphology with state observer algorithm," *IEEE Access*, vol. 12, pp. 12446–12457, 2024, doi: 10.1109/ACCESS.2024.3354790.

[29] F. Mumtaz, K. Imran, H. Rehman, and S. B. A. Bukhari, "Novel protection method for AC microgrids with multiple distributed generations using unscented Kalman filter," *Electric Power Syst. Res.*, vol. 230, May 2024, Art. no. 110227, doi: 10.1016/j.epsr.2024.110227.
[30] A. Srivastava and S. K. Parida, "A robust fault detection and location prediction module using support vector machine and Gaussian process regression for AC microgrid," *IEEE Trans. Ind. Appl.*, vol. 58, no. 1, pp. 930–939, Jan. 2022, doi: 10.1109/TIA.2021.3129982.
[31] F. Mumtaz, K. Imran, H. Rehman, and S. B. A. Bukhari, "1D recursive median filter based passive islanding detection strategy for grid-connected distributed generations network," *IET Renew. Power Gener.*, vol. 17, no. 7, pp. 1731–1746, May 2023, doi: 10.1049/rpg2.12708.
[32] D. B. Tay, "Sensor network data denoising via recursive graph median filters," *Signal Process.*, vol. 189, Dec. 2021, Art. no. 108302, doi: 10.1016/j.sigpro.2021.108302.
[33] T. Gush, S. B. A. Bukhari, R. Haider, S. Admasie, Y.-S. Oh, G.-J. Cho, and C.-H. Kim, "Fault detection and location in a microgrid using mathematical morphology and recursive least square methods," *Int. J. Electr. Power Energy Syst.*, vol. 102, pp. 324–331, Nov. 2018, doi: 10.1016/j.ijepes.2018.04.009.
[34] M. Dodangeh and N. Ghaffarzadeh, "Fault detection, location, and classification method on compressed air energy storages based inter-connected micro-grid clusters using traveling-waves, current injection method, online wavelet, and mathematical morphology," *Int. Trans. Electr. Energy Syst.*, vol. 31, no. 12, Dec. 2021, doi: 10.1002/2050-7038.13190.
[35] K. Saleh, A. Hooshyar, and E. F. El-Saadany, "Fault detection and location in medium-voltage DC microgrids using travelling-wave reflections," *IET Renew. Power Gener.*, vol. 14, no. 4, pp. 571–579, Mar. 2020, doi: 10.1049/iet-rpg.2019.0370.

FAISAL MUMTAZ received the B.S. degree in electrical engineering specializing in power from the University of Wah, Wah Cantt, Pakistan, in 2015, and the M.S. degree in electrical engineering (power) from the U.S.–Pakistan Center for Advanced Studies in Energy, National University of Sciences and Technology (NUST), Islamabad, Pakistan, in 2021, where he is currently pursuing the Ph.D. degree. He was an Instructor with the Electrical Engineering Department, Swedish Institute of Science and Technology, Wah Cantt, from 2017 to 2018. He was honored with a fully funded scholarship by USAID for his master's degree and also awarded with IRSIP Fellowship at Arizona State University by the Higher Education Commission, Pakistan. His research interests include microgrid protection, state estimation, distributed generation, machine learning/artificial intelligence, discrete signal processing, and system identification. He serves as a Reviewer for esteemed journals, such as *Computers and Electrical Engineering* (Elsevier) and *City and Environment Interactions* (Elsevier).

TAHA SAEED KHAN received the B.E. degree in electrical engineering from the National University of Sciences and Technology, Pakistan, in 2015, and the M.Sc. degree in power engineering from the Technical University of Munich, Germany, in 2018. He is currently pursuing the Ph.D. degree in electrical engineering with Oklahoma State University, USA.

MOHAMMED ALQAHTANI (Member, IEEE) was born in October 1989. He received the B.S. degree in electrical engineering from Prince Sattam bin Abdulaziz University, Saudi Arabia, in 2012, the M.S. degree from the University of South Florida (USF), in 2016, and the Ph.D. degree from the USF Smart Grid Power Systems Laboratory, in 2021. He is currently an Assistant Professor with Prince Sattam bin Abdulaziz University. His research interest includes power system computing and modeling.

HADEED AHMED SHER (Senior Member, IEEE) received the B.Sc. degree in electrical engineering from Bahauddin Zakariya University, Multan, Pakistan, in 2005, the M.Sc. degree in electrical engineering from the University of Engineering and Technology, Lahore, Pakistan, in 2008, and the Ph.D. degree in electrical engineering from King Saud University, Riyadh, Saudi Arabia, in 2016. He is currently an Associate Professor with the Faculty of Electrical Engineering, Ghulam Ishaq Khan Institute of Engineering Sciences and Technology, Topi, Pakistan. He has authored and coauthored more than 50 publications in IEEE transactions, journals, and conferences. His research interests include grid connected solar photovoltaic systems, maximum power point tracking, fault analysis of PV systems, and power electronics. He was the recipient of the Research Excellence Award from the KSU College of Engineering in 2012 to 2015. He is an Associate Editor for IET Renewable Power Generation.

ALI S. ALJUMAH was born in July 1989. He received the B.Sc. degree in electrical engineering from the King Fahd University of Petroleum and Minerals (KFUPM), Saudi Arabia, in 2012, and the M.Sc. and Ph.D. degrees in electrical engineering from the University of South Florida (USF), USA, in 2016 and 2022, respectively. Currently, he is an Assistant Professor with the Electrical Engineering Department, Prince Sattam bin Abdulaziz University. His research interests include power systems modeling, stability, and renewable energy sources integration to the power grid.

SULAIMAN Z. ALMUTAIRI was born in March 1988. He received the B.Sc. degree from Prince Sattam bin Abdulaziz University, Al-Kharj, Saudi Arabia, in 2012, and the M.Sc. and Ph.D. degrees in electrical engineering from the University of South Florida, Tampa, USA, in 2016 and 2021, respectively. Currently, he is an Assistant Professor with Prince Sattam bin Abdulaziz University.